



ISSN: 0976-3031

Available Online at <http://www.recentscientific.com>

International Journal of Recent Scientific Research  
Vol. 7, Issue, 9, pp. 13259-13267, September, 2016

**International Journal of  
Recent Scientific  
Research**

## Research Article

### GAIN IN LIFT AND STABILIZATION OF THE AIRFOIL WAKE AT VERY-LOW REYNOLDS NUMBER VIA A TRAILING EDGE FLEXIBLE-FLAP

**Chedhli Hafien\*<sup>1</sup>, Adnen Bourehla<sup>2</sup> and Mounir Bouzaiane<sup>1</sup>**

<sup>1</sup>Laboratory of Mechanics of Fluids, Faculty of Science of Tunis, 1060 Tunis cedex, Belvidère

<sup>2</sup>Aviation School of Borj El-Amri (ASBA), B.P 1142, Tunisia

#### ARTICLE INFO

##### Article History:

Received 06<sup>th</sup> June, 2015

Received in revised form 14<sup>th</sup> July, 2016

Accepted 23<sup>rd</sup> August, 2016

Published online 28<sup>th</sup> September, 2016

##### Key Words:

Flexible-flap, Trailing edge, Flow stabilization, Two-way Fluid-Structure Interaction (FSI).

#### ABSTRACT

The passive control of the unsteady flow around the NACA0012 airfoil at very low Reynolds number ( $Re=1.4 \times 10^3$ ) is studied numerically by using the ANSYS-Workbench software. This airfoil is equipped with a flexible flap attached at the trailing edge.

The resolution of the two-way Fluid-Structure Interaction (FSI) problem was approached by the system coupling service.

The presence of the trailing edge flexible flap has an effect to increase the lift coefficient of about 23% and to reduce the instability coefficient from 54.6% to 36.72%, for an angle of attack of  $20^\circ$ . These ameliorations are caused by the change of the flow characteristics. During its interaction with the surrounding flow, the flap oscillates around an equilibrium position with a dimensionless frequency  $f_0^*=0.458$ , this decreases the Strouhal number of the flow from 0.495 to 0.463. Moreover, the presence of this flap resists the rotation movements of the contra-rotating vortices and translates the second vortex downstream of the trailing edge in the longitudinal direction. This imposes major modifications in the airfoil wake properties, where it will be more stable and narrower.

Copyright © Chedhli Hafien., Adnen Bourehla and Mounir Bouzaian., 2016, this is an open-access article distributed under the terms of the Creative Commons Attribution License, which permits unrestricted use, distribution and reproduction in any medium, provided the original work is properly cited.

## INTRODUCTION

In the recent years, the interest of flight at low Reynolds number is increased in industry and research (Neef and Hummel 2001). The using of micro and nanotechnologies is necessary for many military and civil applications. The Unmanned Aerial Vehicles (UAV) and Micros Aerial Vehicles (MAV) are capable of moving at the closed and narrowed environments, such as the buildings and the tunnels. The UAV and MAV are also employed where the human presence is dangerous or impossible (Venkataraman 2013).

The presence of an airfoil in flow field provokes the creation of two contra-rotating vortices on the extrados and downstream of the trailing edge (Mazellier and Kourta 2011; Hafien *et al* 2013). For the flow at Reynolds number greater than 500, both vortices are detached from the airfoil for an incidence angle of about  $10^\circ$  (Dergham 2007; Bhat and Govardhan 2013). The detachment of these vortices makes the flow unstable and characterized by a Strouhal number  $St=cf/U$  (where  $c$  is the airfoil chord length,  $f$  is the flow perturbation frequency, and  $U$  is the free-stream velocity). The vortex-shedding is formed by the interaction between both vortices in the airfoil wake.

The phenomenon of flight in nature is generally realized at low Reynolds number, started from  $10^3$  for insects to  $5 \times 10^4$  or more

for birds such as eagles. In this laminar regime the presence of vortices on the extrados and downstream of the trailing edge has a harmful effect on the aerodynamic performance (Mueller 2001). The wings in nature are made up of flexible structures, in order to well react with the surrounding flow. This allows it to avoid the harmful effect of the separated flow in the unsteady laminar regime (Frampton *et al* 2001; Chimakurthi and Tang 2009).

In literature, varied researchers studied the separation flow control upper side of the airfoil through the use of auto-adapted flexible structures (Venkataraman and Bottaro 2012; Brücker and Weidner 2014; Bourehla *et al* 2015; Hafien *et al* 2016). Very good results were obtained for high incidence angles. There are modifications of the flow topology at large scale involving important ameliorations of aerodynamic efforts.

In spite of the effectiveness of the auto-activated flaps on the extrados of the airfoil at the high incidence angle, they can play a negative role for low incidence angles, such as the flow perturbation and the decrease of the lift. Fig. 1 (this Figure is imported from Schlüter 2009) shows that when the incidence angle of NACA2213 airfoil varying between  $0^\circ$  and  $10^\circ$ , the lift coefficient decreases under the effect of the auto-activated flap that is attached on the extrados. Similar results are observed in Johnston *et al* (2011).

\*Corresponding author: Chedhli Hafien

Laboratory of Mechanics of Fluids, Faculty of Science of Tunis, 1060 Tunis cedex, Belvidère

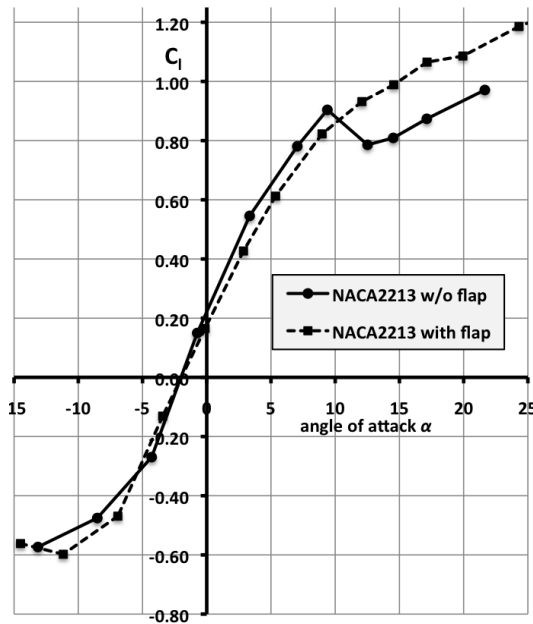


Figure 1 Decrease of the lift coefficient during the presence of an auto-activated flap on the upper side of the NACA2213 airfoil at low incidence angle, (Figure imported from Schlüter 2009).

The active control of the flow downstream of the trailing edge is studied in varied investigations in literature. For example, the Gurney flap is used in order to increase the lift coefficient of the airfoil (Giguère 1997). But, the installation of this flap perpendicularly to the flow provokes the increase of the instability of the wake downstream of the trailing edge, which increases the drag coefficient (Houghton and Carpenter 2006). This problem is among the inconveniencies of the Gurney flap. In order to avoid the negative role of the auto-activated flap that is placed on the extrados of the airfoil at the low incidence angle, and to remedy the increase of drag coefficient provoked by Gurney flap, we propose a new type of auto-activated flexible flap attached at the airfoil trailing edge, parallel with the flow. This problem of Fluid-Structure Interaction is numerically investigated by the ANSYS-Workbench. In the first section, we present the numerical model that describes the coupling between the fluid flow and the flexible flap. The instability study of flow at low Reynolds number  $Re=1.4 \times 10^3$ , around the NACA0012 airfoil (without control) at different angles  $\alpha$  ( $\alpha$  varying between  $0^\circ$  and  $20^\circ$ ), is presented in the second section. For  $\alpha=20^\circ$ , we have presented a frequential and structural analysis in order to specify the relation between the flow topology and the aerodynamic efforts. Finally, the effect of the presence of the trailing edge flexible flap on the flow topology and on the aerodynamic efforts is studied in the last section.

### Numerical Model

In this section, we present the numerical model of the two-way coupling between the unsteady flow and the flexible flap. There are two independent computational domains: the fluid domain and the structure domain (flap). Each domain is defined by its proper geometry, physical properties, mesh, boundary conditions, and equations. Each domain was simulated in its proper solver. Consequently, the coupling between both solvers is realized in order to simulate the two-way FSI.

### Geometries, boundary conditions and meshes

We consider a symmetric NACA0012 airfoil equipped with trailing edge flexible flap (see Fig. 2 (a)), placed in an airflow filed at very low Reynolds number  $Re=1.4 \times 10^3$ .

This problem is numerically studied using the commercial code ANSYS-Workbench. The geometries of Fluid and Structure (flap) domains are modeled by using the « DesignModeler » system and then exported respectively to « CFD-Fluent » and « Transient Structural » systems. The fluid domain consists of  $10c$  upstream,  $15c$  downstream and  $10c$  in the top and bottom of the airfoil. The domain's width is equal to  $0.1c$ . The boundary conditions of the fluid domain are: "Wall" for the airfoil and the interfaces surrounding the flap (see Fig. 2 b), "Inlet" for the input condition and for the upper and lower borders, "Outlet" for output condition, and "Symmetry" in the borders according to the span. The fluid domain meshes with a structural block grid. This grid contains 72000 cells. The near-wall cells are tightened and refined in order to hold account the pressure and speed gradients, see Fig. 3 b. In order to study the auto-movement of the flap, the dynamic mesh model is employed. We only use the smoothing method. The dynamic mesh regions are defined as following:

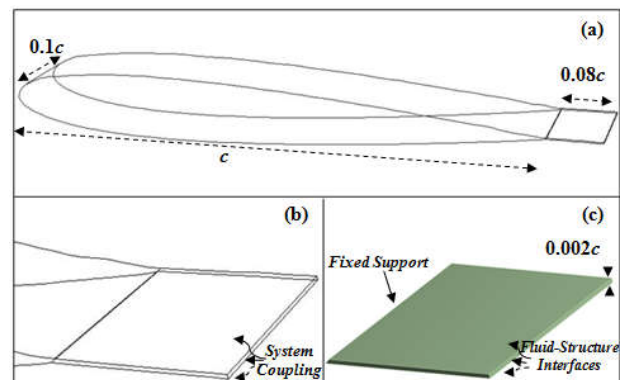


Figure 2 (a) NACA 0012 airfoil equipped with flexible flap at the trailing edge (Fluid domain); (b) Zoom: interfaces surrounding the flap (Fluid domain); (c) flexible flap (Structure domain).

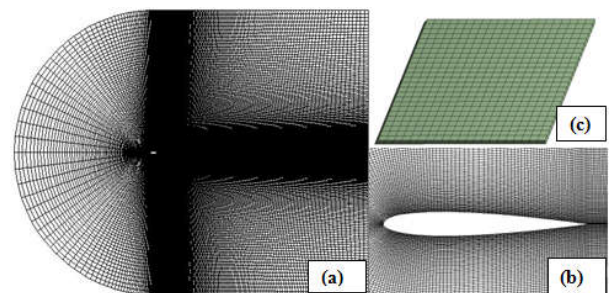


Figure 3 Mesh of the Fluid domain (ANSYS-Fluent) (a) and (b). Mesh of the flap (ANSYS-Mechanical) (c).

- Airfoil, inlet and outlet borders: "Stationary"
- Interfaces surrounding the flap: "system coupling", see Fig. 2 b
- Borders according to the span: "Deforming".
- The Structure domain consists of  $0.08c$ ,  $0.002c$  and  $0.1c$  as length, thickness, and width of the trailing edge flexible flap (see Fig. 2). The boundary conditions of the flexible flap are (see Fig. 2c):
- Fixed support: for the flap root

- Fluid Structure Interfaces: for the extrados, intrados and trailing edge of the flap.

This domain is divided into numbers of elements. There is a structural mesh made up of 3908 nods and 525 elements, see Fig. 3 c.

**Equations**

The continuity (1) and momentum (2) equations that describe the incompressible fluid flow (Liaw 2005) are:

$$\frac{\partial u_i}{\partial x_j} = 0 \tag{1}$$

$$\frac{\partial u_i}{\partial t} + u_j \frac{\partial u_i}{\partial x_j} = -\frac{1}{\rho} \frac{\partial p}{\partial x_i} + \frac{\partial}{\partial x_j} \left( \nu \frac{\partial u_i}{\partial x_j} \right) \tag{2}$$

Where:  $u$  is the flow velocity,  $P$  is the pressure,  $\rho$  is the fluid density and  $\nu$  is the kinematic viscosity.

According to the Reynolds number, the flow is laminar. The numerical resolution of these equations in the Fluent solver is realized directly by using the Finite Volume Method (FVM). The discretization scheme used is « second order upwind ». The algorithm used for the coupling between the pressure and the velocity is PISO; this algorithm is famous for the flow with the important pressure gradient.

Concerning the structure domain, the deformation of the flexible flap is defined by the Hooke equation (3):

$$\sigma_{ij} = 2\bar{\mu}\varepsilon_{ij} + \bar{\lambda}\varepsilon_{kk}\delta_{ij} \tag{3}$$

Where:  $\sigma_{ij}$  is the stress tensor,  $\bar{\mu}$  and  $\bar{\lambda}$  are the Lamé coefficients, and  $\varepsilon_{ij}$  and  $\delta_{ij}$  are respectively the deformation and unit tensors.

For a structure made up of homogenous and isotropic material, the Lamé coefficients  $\bar{\mu}$  and  $\bar{\lambda}$ , are defined as functions of Young’s modulus  $E$  and Poisson coefficient  $\bar{\nu}$  (Gaugain 2014), see equations (4):

$$\bar{\lambda} = \frac{E\bar{\nu}}{(1+\bar{\nu})(1-2\bar{\nu})} ; \bar{\mu} = \frac{E}{2(1+\bar{\nu})} \tag{4}$$

The density, Young’s modulus and Poisson coefficient of the flap are respectively:  $\rho_{vlr}=10^3\text{g.m}^{-3}$ ,  $E = 5 \times 10^5\text{Pa}$ , and 0.35.

The equations describing the transient deformation of the flexible flap are numerically resolved via the “Transient Structural” solver by using the Finite Element Method (FEM).

**System coupling**

The interaction problem between the fluid flow and the trailing edge flexible flap is numerically studied by the coupling between the “CFD-Fluent” and “transient Structural” Solvers. The Fluent solver computes the fluid pressure surrounding the flap, and the “Transient Structural” solver determines the deformation of the flap under the effect of the flow pressure. This deformation affects the state of the surrounding fluid, for this reason, the Fluent solver updates the mesh of the fluid domain and then the pressure is recomputed again. Thus, there is a two-way Fluid-Structure Interaction.

The co-simulation of both solvers is realized under the management of the coupling system service. All necessary data for this coupling are transformed through the interfaces between Fluid and Structure Domains. These interfaces are defined as ‘system coupling’ in « CFD-Fluent » and ‘Fluid-Structure Interfaces’ in « Transient Structure », sees Fig. 2 (b) et (c).

**RESULTS**

**Flow around the classical NACA0012 airfoil**

**Study of the flow instability Food effect**

In this section, we have studied the flow around the NACA0012 airfoil at different incidence angles  $\alpha$ . The Reynolds number based on the chord length is equal to  $1.4 \times 10^3$ . Fig.4 presents the evolution of the lift coefficient as a function of the angle of incidence  $\alpha$  ( $\alpha$  varies from  $0^\circ$  to  $25^\circ$ ). The values obtained by ANSYS-Fluent are time-averaged values. A good agreement is obtained between the present results and the results from literature (Soueid et al 2009). This figure shows that the lift coefficient increases proportionally for  $\alpha$ . We note that the increase rate of the lift coefficient is decreased for  $\alpha=10^\circ$  and  $\alpha=20^\circ$ .

The transition of the flow from the stable to the unstable regime is influenced by two terms: the angle of incidence  $\alpha$  and the Reynolds number. The adverse pressure gradient appears when the angle  $\alpha$  increases. This results in the production of two contra-rotating vortices on the upper side and downstream of the trailing edge of the airfoil. Once these vortices are detached from the boundary layer, the flow will be unsteady. The interaction between them in the wake region creates the vortex shedding. For  $Re > 0.5 \times 10^3$ , the instability of the laminar flow is realized from an attack angle of about  $10^\circ$  (Dergham 2007; Bhat and Govardhan (2013)). This explains the decrease of the lift increase rate at  $\alpha=10^\circ$  for  $Re=1.4 \times 10^3$  in our case, see Fig. 4.

Fig. 5 shows the presence of two contra-rotating vortices around the NACA0012 airfoil at different angles. For  $\alpha=5^\circ$  both vortices are attached to the boundary layer. However, for  $\alpha \geq 10^\circ$  these vortices are detached, which shows that the flow is unstable.

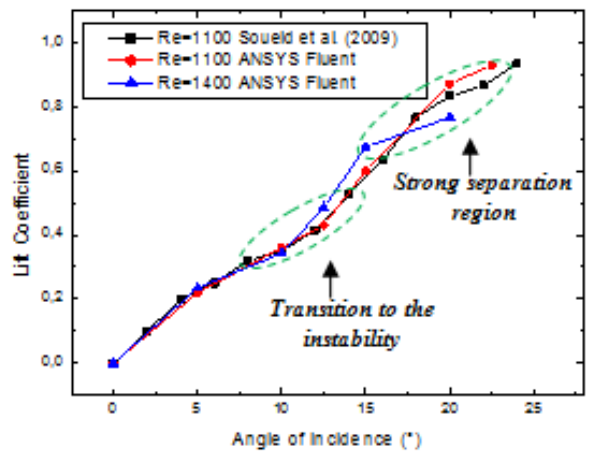


Figure 4 Evolution of the lift coefficient as a function of the angle of incidence of the classical NACA 0012 airfoil.

Fig. 6 (a) and (b) show respectively the evolution of the instability coefficient and the Strouhal number according to the

incidence angle (the instability coefficient is defined as the ratio of amplitude/time-averaged value of the lift coefficient signal). This figure shows that the flow remains unsteady starting from  $\alpha=10^\circ$ . The instability of the flow increases proportionally to  $\alpha$ . However, the Strouhal number evolution is inversely proportional to  $\alpha$ . This shows that the more the flow is unstable, the lower the Strouhal number is.

The sizes of both contra-rotating vortices increase during the increase of the incidence angle. In the post-stall regime, the presence of a greatly separated flow region has a negative effect on the aerodynamic efforts which explains the decrease of the lift increase rate at  $\alpha=20^\circ$ .

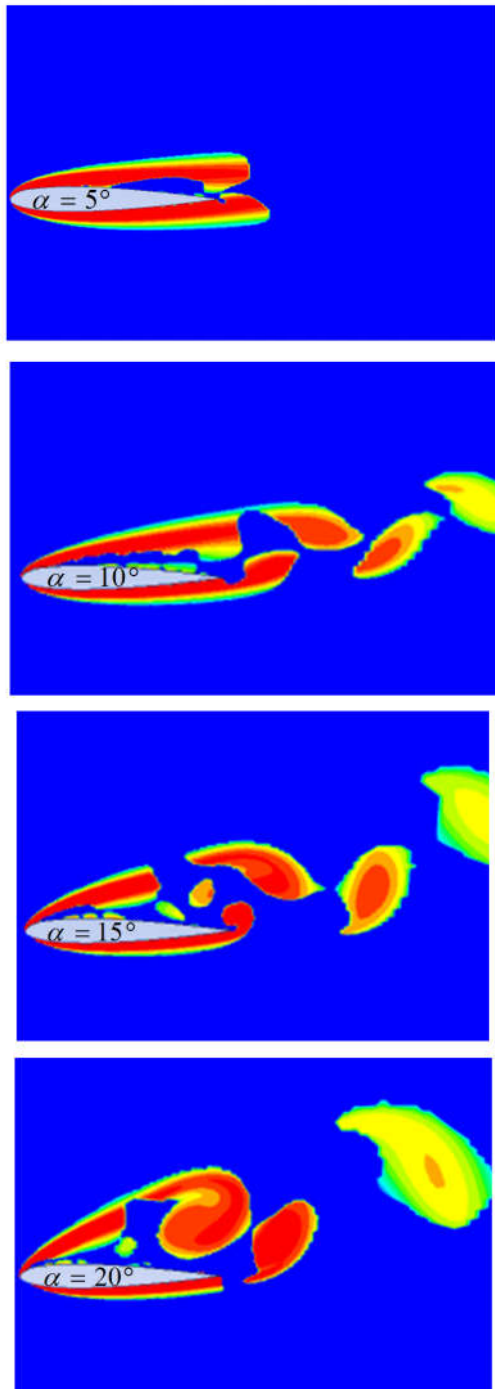


Figure 5 Detachment of the contra-rotating vortices from the airfoil for  $\alpha \geq 10^\circ$ .

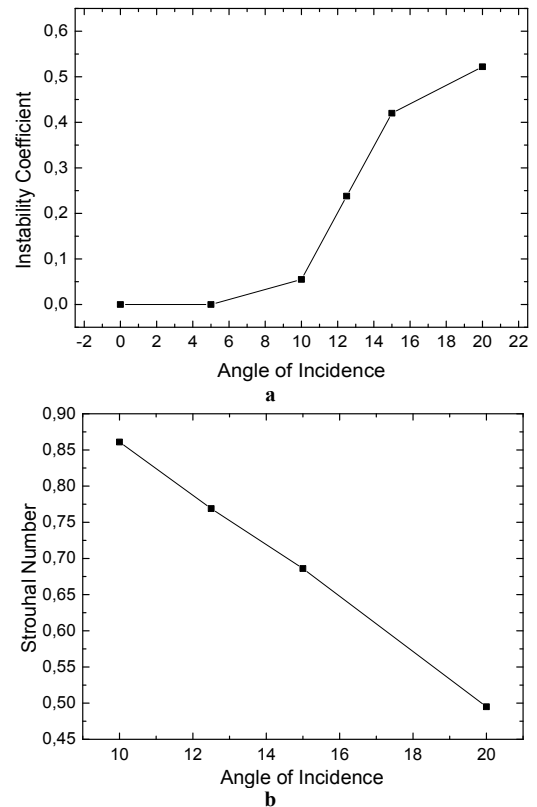


Figure 6 Evolution of the instability coefficient (a) and the Strouhal number (b) as functions of the incidence angle.

#### Characteristics of the aerodynamic effort signals for $\alpha=20^\circ$

For  $\alpha=20^\circ$ , the drag and lift coefficient signals and their FFT, are presented respectively as functions of the dimensionless time  $t^*=t/Uc$  (where;  $t$  is the time) and the Strouhal number. The lift coefficient signal oscillates with an amplitude of 0.415 and with a time-averaged value of 0.76. Thus, it is characterized by an instability coefficient of 54.6%, see Fig. 7 (a). This shows that the flow is strongly unstable. Also, the drag coefficient is strongly unstable, such as its instability coefficient is about 28.75% (0.111 and 0.386 are respectively the amplitude and the time-averaged value of the oscillation of the drag coefficient signal).

Both aerodynamic effort signals vary periodically as functions of the dimensionless time  $t^*$  with a dimensionless period  $T^*$  ( $T^*=TU/c$ ) equal to 2.02. Thus, the flow is dominated by a principal Strouhal number  $St_0=0.495$ . The frequential analysis shows the deformable characteristics of the aerodynamic effort signals. Indeed, the FFT curve shows that the flow is dominated by a secondary Strouhal number  $St_1=0.962$  (see Fig. 7 (b)).

#### Relation between the aerodynamic efforts and the flow topology for $\alpha=20^\circ$

The vorticity field consists by two contra-rotating vortices: the principal vortex that is created on the extrados starting from the leading edge, and the secondary that is created downstream of the trailing edge. Both vortices displace with rotation and translation movements; the rotation is in the hourly sense for the principal vortex and in the trigonometric sense for the secondary vortex, and the translation is in the free-stream flow

direction. After generation and during its movement, the size of each vortex increases, this results in the detachment of the flow from the airfoil and the creation of the vortex shedding in the wake region.

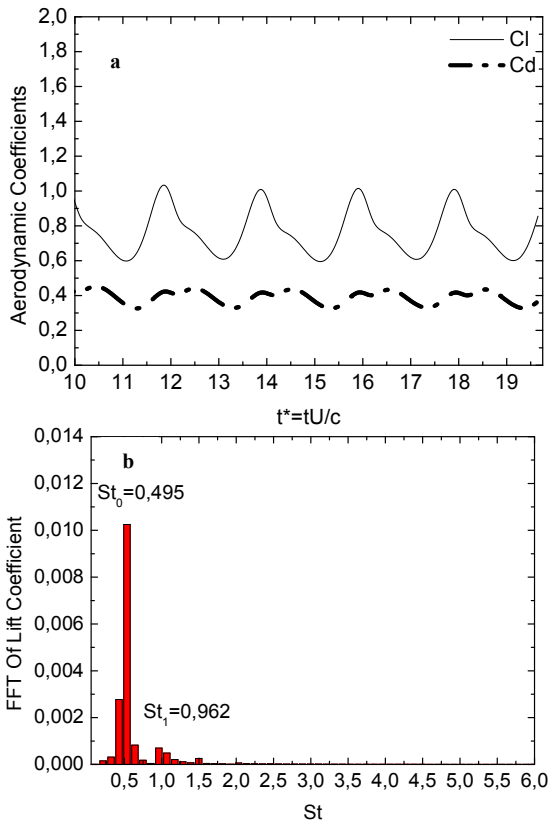


Figure 7 (a) Signals of the lift and drag coefficients as functions of the dimensionless time. (b) FFT of lift coefficient signal, for  $\alpha=20^\circ$

The relation between the vorticity field and the evolutions of aerodynamic efforts, during one temporal period ( $t'=t/T$  varied from 0 to 1; where T is the temporal period of flow), is presented in Fig. 8.

In the beginning of each temporal period ( $0 < t' < 0.19$ ), there is only the principal vortex V(I) that is created on the extrados of the airfoil. This vortex is made up of two components: V1(I) and V2(I) that are sited respectively near the leading edge and in the suction zone of the airfoil. In this temporal interval, the size of V(I) is increasing, and the lift and drag coefficients also increase.

At the moment  $t'=0.19$ , the two components of the principal vortex V1(I) and V2(I) are detached of each other at the level of about  $(0.5c \times \sin\alpha; 0.5c \times \cos\alpha)$ . At the same time, we note the creation of the secondary vortex V(II) downstream of the trailing edge. Besides, the increase of the lift and drag coefficients is stopped under the effect of the new situation of V(I) and V(II).

For  $t' \in [0.19; 0.32]$ , the vortex V2(I) dilates in the longitudinal direction. Then, it decomposes into two elements V'2(I) and V''2(I) at  $t'=0.32$ . This decomposition is caused by the presence of the second vortex V(II). Indeed, both components V'2(I) and V''2(I) were sited respectively upstream and downstream of V(II); moreover, they move away from each other during the increase of its size (size of V(II)). We

note, on another hand, that  $t'=0.32$  is proportional to the time when the decrease of the drag coefficient is stopped.

At the moment  $t'=0.37$  which is corresponding to the first inflexion point in lift coefficient curve, the vortex V'2(I) attaches again to the vortex V1(I). This attachment makes the principal vortex of the extrados characterized by a very large size  $(V(I) = V1(I) + V'2(I) + V''2(I))$ . As the time progresses, the vortex V''2(I) is moving in the longitudinal direction and then detaches from the extrados (at level of  $(x=lc \times \sin\alpha; y=lc \times \cos\alpha)$  where; x and y are respectively the longitudinal and transversal coordinates) at  $t'=0.53$ , and will be one of the components of the NACA0012 airfoil wake. At this moment, the drag coefficient reaches its maximal value and starts to decrease. We also note that the vortices V1(I) and V'2(I) are mixed at this moment, resulting so the vortex V12(I). The vortex V2(I) appears again at  $t'=0.80$  which is corresponding to the minimal value of the lift coefficient.

The size of the secondary vortex V(II) that is produced downstream of the trailing edge, increases along the time interval  $[0.19; 0.90]$ . Because of its translation movement and its size increase, this vortex detaches from the airfoil at  $t'=0.90$ , thus, it joins the wake region. At this moment, the drag coefficient reaches its minimal value and starts increasing.

**Flow around the NACA0012 airfoil equipped with a flexible flap placed at the trailing edge**

In this section, we study the control of the vortex V(II) that is created downstream of the trailing edge of the NACA0012 airfoil via an auto-activated flexible flap. The physical and geometrical characteristics of this flap are presented in the last section (§Numerical model).

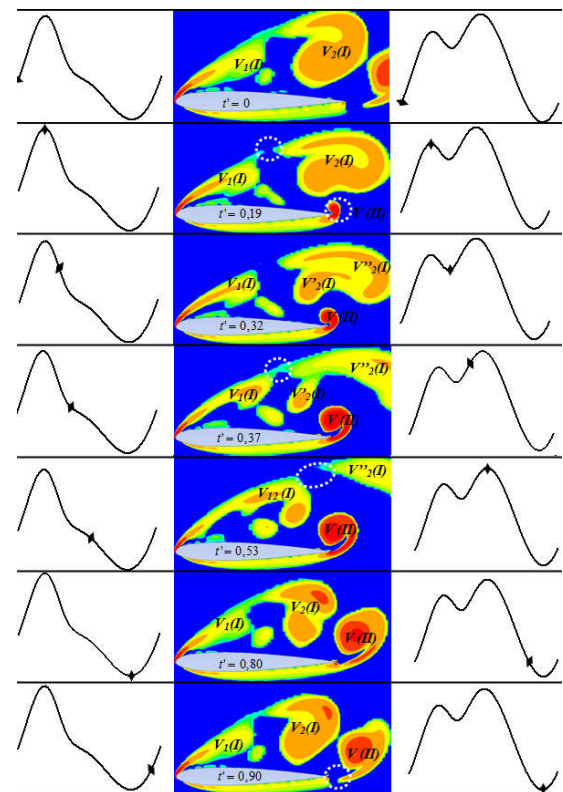


Figure 8 Relation between the evolutions of the vorticity field (middle) and the aerodynamic efforts during one period: (left) lift coefficient; (right) drag coefficient.

**Flow stabilization and decrease of the lift coefficient**

Fig. 9 presents the evolution of time-averaged lift coefficient according to the incidence angle  $\alpha$  for the controlled and uncontrolled cases. For  $\alpha \leq 5^\circ$ , the flap has not any effect on the aerodynamic performances. For the high incidence angles, the lift coefficient is significantly improved. Its maximum increase is obtained for  $\alpha=20^\circ$ .

The presence of the flexible flap at the airfoil trailing edge stabilizes the fluid flow, especially for the high incidence angle. Indeed, the instability coefficient is significantly decreased in the controlled case. This decrease is more important when the incidence angle is higher. The maximum decrease of the instability coefficient is obtained for  $\alpha=20^\circ$ , see Fig. 10 (a). Fig. 10 (b) shows that the Strouhal number decreases under the effect of the presence of the flap.

Fig. 11 (a) and (b) show respectively the signals of the lift and drag coefficients as functions of the dimensionless time  $t^*$  for  $\alpha=20^\circ$ . There are periodic curves with a dimensionless temporal period  $T^*=2.15$  corresponding to a principal Strouhal number  $St'_0=0.463$ . The lift coefficient signal is characterized by a time-averaged value equal to 0.94 and amplitude equal to 0.345. Thus, the lift coefficient after control is increased by about 23%, and the instability coefficient is decreased from 54.6% to 36.72%. However, the amplitude and the time-averaged value of drag coefficient will not have any important modification compared to the case without control.

The frequential analysis shows that the lift and drag coefficients are characterized as deformable signals. Indeed, the FFT curves approve the appearance of the second peak, which shows that the flow is dominated by a secondary Strouhal number  $St'_1=0.926$ . Fig. 11 (c) and (d) prove that the principal and secondary Strouhal numbers in the uncontrolled case are greater than that in the controlled case. This is caused by the increase of the dimensionless temporal period  $T^*$  from 2.02 to 2.16.

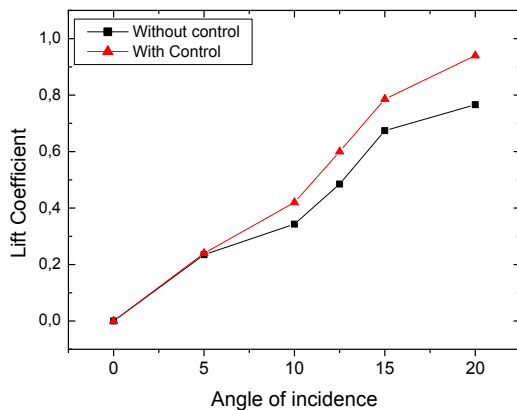


Figure 9 Evolution of the lift coefficient as a function of the incidence angle in the uncontrolled and controlled cases.

**Modification of the flow topology at large scale**

Fig. 12 presents the pressure contour around the airfoil in the controlled case at  $t^*=0.00, 0.17, 0.45$  and  $0.80$  corresponding respectively to the beginning of the period, Cl-maximum, Cl-medium, and Cl-minimum. We note the creation of two low-pressure regions upper side and downstream of the trailing

edge of the airfoil. This provokes the production of the two contra-rotating vortices.

The presence of the auto-activated flexible flap at the trailing edge affects the global structure of the flow. Indeed, the second region of low pressure is translated from airfoil trailing edge to the flap extremity. This translation gives more space to the principal low-pressure region to dilate on the airfoil extrados before being detached, see Fig. 12.

Fig. 13 presents the evolution of the flow field during a cycle. By comparison between the controlled and uncontrolled cases, we note that the interaction between the flexible flap and the flow downstream of the trailing edge changes the characteristics of the vortices field that consists of the principal vortex V(I) and the secondary vortex V(II).

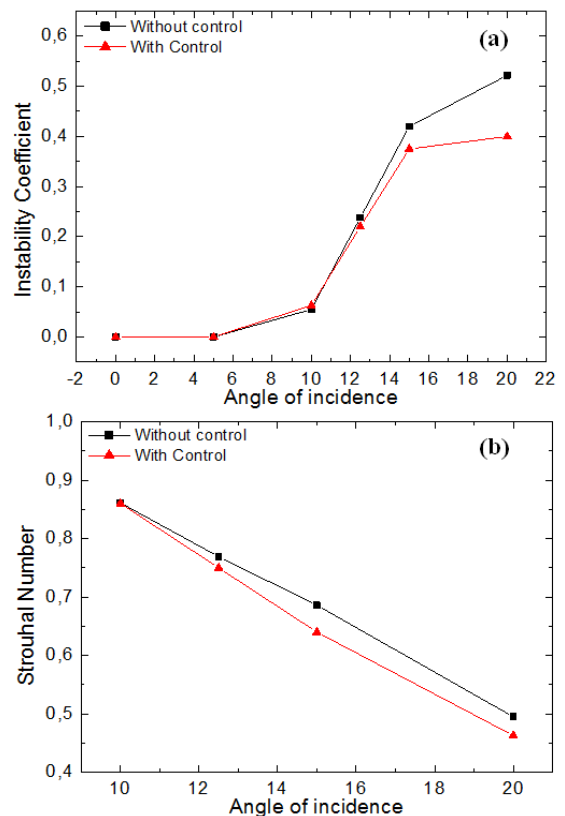


Figure 10 Evolution of the instability coefficient (a) and the Strouhal number (b) as functions of the incidence angle, in the uncontrolled and controlled cases.

At the beginning of the period  $[0.00; 0.17]$ , there is no change of the flow topology compared to the uncontrolled case, where only the vortex V(I) exists on the upper side of the airfoil ( $V(I)=V1(I) + V2(I)$ ). At  $t^*=0.17$ , both components of the principal vortex V1(I) and V2(I) are detached from each other, and the secondary vortex V(II) is created. This latter is clearly translated from the airfoil trailing edge in the uncontrolled case to the flap extremity in the controlled cases.

Similarly to the uncontrolled case, at  $t^*=0.34$  the vortex V2(I) is decomposed into two elements  $V'2(I)$  and  $V''2(I)$  under the effect of the presence of V(II). This latter (V(II)) is detached from the airfoil at  $t^*=0.47$ , but it remains still attached to the flexible flap. This helps the principal vortex to dilate in the longitudinal direction and to gain more time before the

detachment between its components  $V^2(I)$  and  $V^2(II)$ . Indeed, the vortex  $V^2(II)$  is detached from the airfoil and joins the wake region at  $t^*=0.53$  at the level of  $x=1c \times \sin\alpha$  in the uncontrolled cases, however, during the presence of the flexible flap, this vortex is detached at  $t^*=0.68$  at the level of about  $x=1.08c \times \sin\alpha$  (see Fig.13).

We also note that the rotation frequency of both vortices  $V(I)$  and  $V(II)$  decreases significantly in the controlled case compared to the uncontrolled case (see Fig. 13 and Fig. 14). This shows that the automatic oscillation of the flexible flap under the effect of the interaction with the surrounding flow resists the rotation movement of  $V(II)$  which also affects the

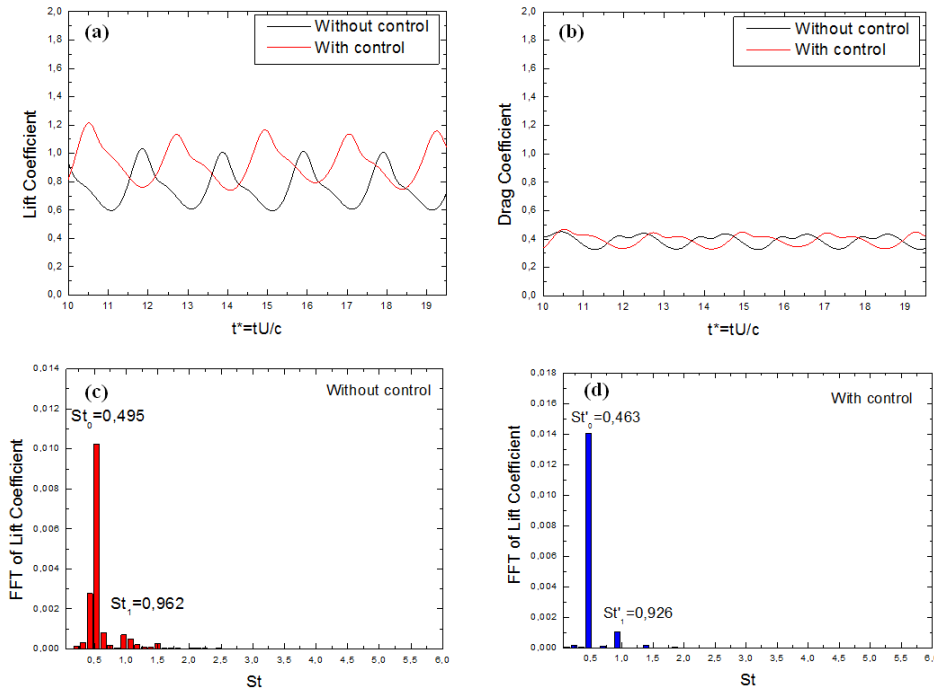


Figure 11 Signals of the lift (a) and drag (b) coefficients for the uncontrolled and controlled cases; FFT of the lift coefficient for the uncontrolled (c) and controlled (d) cases.

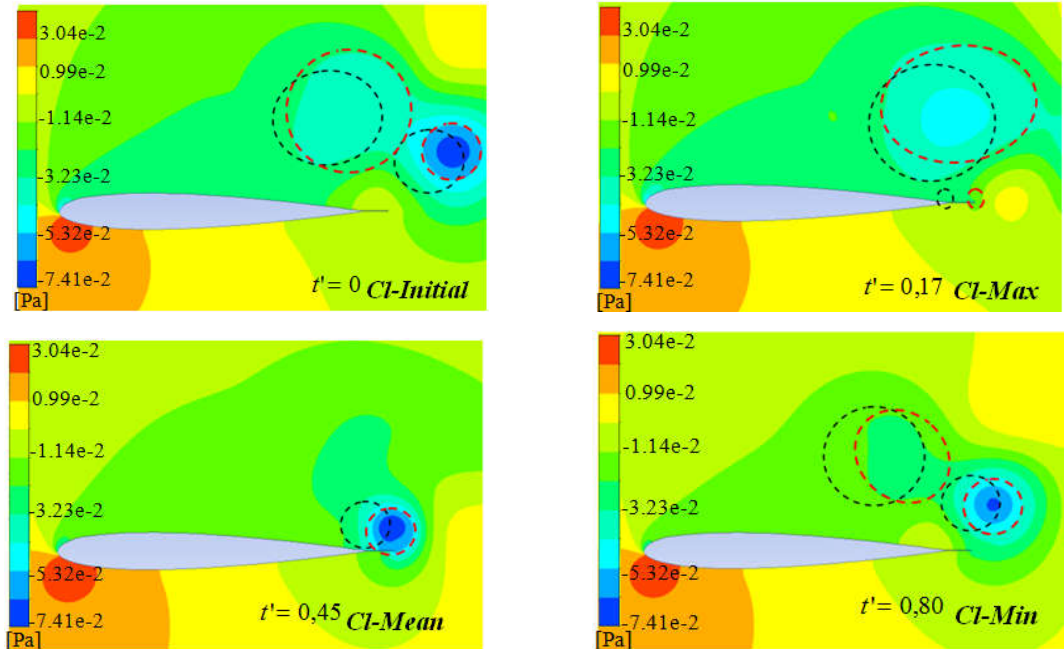
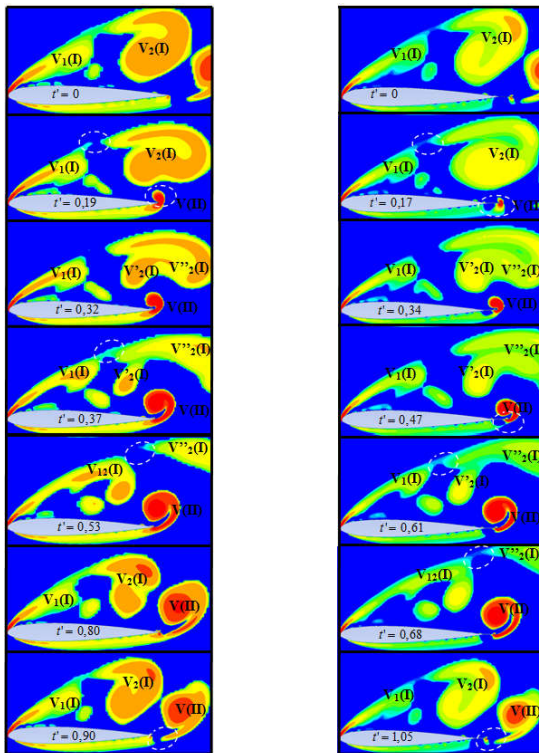


Figure 12 Pressure contour around of the NACA0012 airfoil in the controlled case at different critical times. (Black circles) without control; (red circles) with control.

The second vortex  $V(II)$  detaches from the flap extremity and will be one of the components of the airfoil wake at  $t'=1.05$ . This physical phenomenon is repeated when  $t'$  reaches the value 1.07. Thus, the flexible flap plays a role of dilating the temporal period.

Fig. 14 presents the vortex shedding in the wake region behind the NACA0012 airfoil without and with control. Major modifications are observed under the effect of interaction between the flexible flap and the secondary vortex. We can summarize these modifications into three points described below:



**Figure 13** Cycle of evolution of the vorticity Field around of the NACA0012 airfoil in the uncontrolled (left) and controlled (right) cases.

- The rotation frequency of both contra-rotating vortices significantly decreases under the effect of the resistance of the flexible flap. So, the wake region remains less perturbed and more stable.
- The size of each vortex was reduced when it moves away from the airfoil under the effect of the decrease of its angular velocities. Consequently, a reduction of the wake thickness far from the airfoil is obtained.
- The principal and secondary vortices move away from each other because of the decrease of the Strouhal number (an increase of the temporal period). Thus, the wake region prolongs in the longitudinal direction.

These modifications in the wake region characteristics (more stable, narrower...) result in the amelioration of the lift coefficient of about 23%.

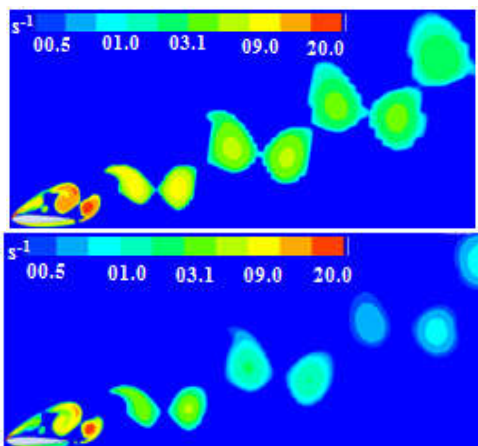


**Figure 14** Vortex shedding in the wake region behind of the NACA0012 airfoil; (top) without control; (bottom) with control.

**Relation between the flap oscillation and the flow topology**

During its interaction with the secondary vortex, the trailing edge flexible flap oscillates around an equilibrium position. Fig.15 presents the instantaneous deformation of this flap under the effect of the flow pressure force. The flap oscillation (vertical coordinate of the flap extremity) as a function of dimensionless time  $t^*$  is presented in Fig. 16 (a). This figure shows that the deformation varies periodically with a dimensionless temporal period equal to 2.18.

In spite of its low oscillation amplitude, the flexible flap has a great effect on the flow topology. Fig. 16 (b) presents the FFT of the flap oscillation curve. This figure shows that the flap deformation is dominated by an only one dimensionless frequency  $f_0^*=0.458$ . By comparing this frequency with the Strouhal numbers in the uncontrolled ( $St_0$ ) and controlled ( $St'_0$ ) cases, we prove that  $f_0^* < St'_0 < St_0$ . This shows that the flap imposes a certain resistance to the flow, which changes the characteristics of the wake behind the airfoil. These modifications affect the aerodynamic efforts by increasing the lift coefficient.

Therefore, on the one hand, the flap affects the flow by decreasing the Strouhal number from  $St_0=0.495$  to  $St'_0=0.463$  and by modifying the wake region characteristics, and on the other hand, the flow affects the flap by modifying its state from the stability to the deformation with a dimensionless frequency  $f_0^*=0.458$ . There is also a two-way Fluid-Structure Interaction.

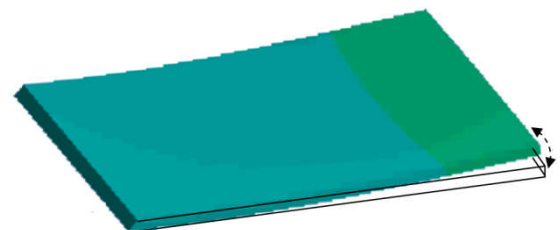


**Figure 15** Instantaneous deformation of the flexible flap under the effect of the pressure force of the flow

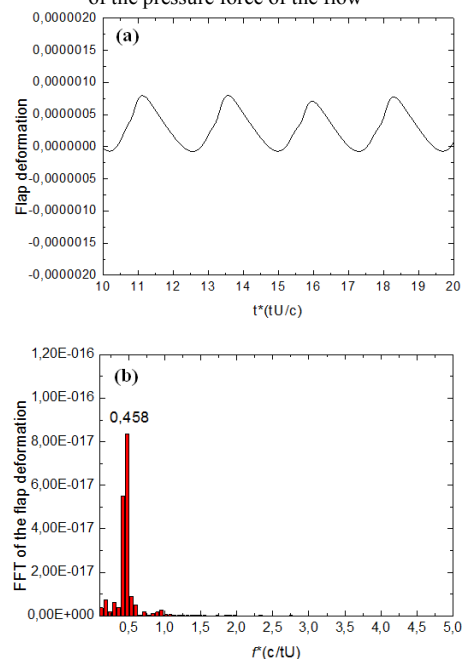


**Figure 16** (a) Deformation of the flap as a function of dimensionless time  $t^*$ ; (b) FFT of the flap deformation.

## CONCLUSION

In this paper, we numerically studied by using the ANSYS-Workbench, the control of flow at very low Reynolds Number ( $Re=1.4 \times 10^3$ ) around the NACA0012 airfoil equipped with a trailing edge flexible flap. The two-way fluid-structure interaction problem is approached by coupling between “CFD-Fluent” and “Transient Structural” systems.

The instability of the flow around the classical NACA 0012 airfoil (without control) is investigated for different angles of incidence  $\alpha$  ( $\alpha$  varies from  $0^\circ$  to  $20^\circ$ ). For the high incidence angle ( $\alpha=20^\circ$  in the post-stall regime), a structural and frequential analysis is presented in order to determine the relationship between the aerodynamic efforts and the flow topology.

The presence of the trailing edge flexible flap has an effect of stabilizing the flow and improving the lift coefficient when the incidence angle  $\alpha$  is greater than  $5^\circ$ . The lift coefficient won't be modified significantly. The maximal increase of the lift coefficient that is obtained for  $\alpha=20^\circ$  is about 23%. Also, the maximal decrease of the instability coefficient from 54.6% to 36.72% is obtained for  $\alpha=20^\circ$ .

The improvement of the lift coefficient and the stabilization of flow were provoked by the modification of the flow characteristics. Indeed, during of its interaction with the surrounding fluid, the flap oscillates around an equilibrium position with a dimensionless frequency  $f_0^*=0.458$  which reduces the Strouhal number from 0.495 to 0.463. Similarly, the presence of this flap resists the rotation movements of both contra-rotating vortices and translates the secondary vortex downstream of the trailing edge. This imposes major modifications on the properties of the wake behind the airfoil, where it remains more stable and narrower.

## References

- Bhat S. S. and Govardhan R. N. (2013): Stall flutter of NACA 0012 airfoil at low Reynolds numbers. *Journal of Fluids and Structures* 41 (2013) 166–174
- Bourehla, A., Hafien, C. and Lili, T., (2015). Simulation numérique de l'interaction fluide structure d'un profil d'aile équipé de volets élastiques. 22ème Congrès Français de Mécanique, Lyon, 24 au 28 Août 2015.
- Brucker C. and Weidner C.: Influence of Self-adaptative hairy flaps on the stall delay of an airfoil in ramp-up motion, *Journal of Fluids and Structures* 47 (2014) 31-40.
- Chimakurthi S. K. and Tang J.: Computational Aero-elasticity Framework for Analyzing Flapping Wing Micro Air Vehicles. *Aiaa Journal* Vol. 47, No. 8, August 2009
- Dergham G. (2007): Etude de la stabilité du lâcher tourbillonnaire d'un profil NACA 0012, Projet de fin d'études, Université Pierre et Marie Curie, Paris,
- Frampton, K. D., Goldfarb, M., Monopoli, D., and Cveticanin, D., Passive Aeroelastic Tailoring for Optimal Flapping Wings,” Fixed and Flapping Wing Aerodynamics for Micro Air Vehicle Applications, edited by T. J. Mueller, Vol. 195, Progress in Astronautics and Aeronautics, AIAA, Reston, VA, 2001, pp. 473–482.
- Gaugain F. 2014: Analyse expérimentale et simulation numérique de l'interaction fluide-structure d'un hydrofoile élastique en écoulement sub-cavitant et cavitant. Thèse de doctorat Mechanics 2014 [physics.med-ph]. Ecole nationale supérieure d'arts et métiers - ENSAM, 2013. French. <NNT: 2013ENAM0054> <pastel-00939286>.
- Giguère P., Dumas G. and Lemay J.: Gurney flap scaling for optimum lift-to-drag ratio. *AIAA Journal*, 35(12):1888-1890, 1997.
- Hafien C.; Bourehla A. and Bouzaiane M.: Passive Separation Control on a Symmetric Airfoil via Elastic-Layer. *Journal of Applied Fluid Mechanics*, Vol. 9, No. 5, pp. 2569-2580, 2016..
- Hafien C., Bourehla A., Lili T. 2013: Simulation numérique d'un écoulement autour d'un profil d'aile muni d'un volet poreux”; 21ème Congrès Français de Mécanique, Bordeaux 26 au 30 août 2013.
- Houghton E.L. and Carpenter P.W.: Aerodynamics for engineering students. Elsevier Publications, 2006.
- Johnston J., Gopalarathnam A., and Jack R. Edwards, Jr. 2011: Experimental Investigation of Bio-Inspired High Lift Effectors on a 2-D Airfoil. 29th AIAA Applied Aerodynamics Conference 27 - 30 June 2011, Honolulu, Hawaii.
- Liaw K. F. 2005: Simulation of Flow around Bluff Bodies and Bridge Deck Sections using CFD. PhD, University of Nottingham, June 2005.
- Mazellier, N. and Kourta, A. (2011). Amélioration des performances aérodynamiques d'un profil au moyen d'un actionneur passif auto-adaptatif. 20ème Congrès Français de Mécanique Besançon, 29 août au 2 septembre.
- Mueller, T.J.a.D., J.D. (2001). An Overview of Micro Air Vehicle Aerodynamics, in Fixed and Flapping Wing Aerodynamics for Micro Air Vehicle Applications. AIAA, Progress in Astronautics and Aeronautics, p. 1-10.
- Neef M.F. and Hummel D. (2001): Euler Solutions for a Finite-Span Flapping Wing. Conference on Fixed, Flapping and Rotary Wing Aerodynamics at very Low Reynolds Number, edited by T.J. Mueller, Vol. 195, pp. 429-451.
- Schlüter J. U. 2009: Lift Enhancement at Low Reynolds Numbers using Pop-Up Feathers. 39th AIAA Fluid Dynamics Conference 22 - 25 June 2009, San Antonio, Texas.
- Soueid H., Guglielmini L, Airiau C. and Bottaro A.: Optimization of the motion of a flapping airfoil using sensitivity functions. *Comput. Fluids*, 38:861-874, 2009
- Venkataraman, D. and Bottaro, A. (2012): Numerical modeling of flow control on a symmetric aerofoil via a porous, compliant coating. *Physics of Fluids*, 24, 093601.
- Venkataraman D. 2013: Flow control using a porous, compliant coating of feather-like actuators. Phd thesis, University of Genova, Italy, 2013.

\*\*\*\*\*